



**HAL**  
open science

# A class of morphing shell structures satisfying clamped boundary conditions

Matteo Brunetti, A. Vincenti, S. Vidoli

► **To cite this version:**

Matteo Brunetti, A. Vincenti, S. Vidoli. A class of morphing shell structures satisfying clamped boundary conditions. *International Journal of Solids and Structures*, 2016, 82, pp.47-55. 10.1016/j.ijsolstr.2015.12.017 . hal-01259914

**HAL Id: hal-01259914**

**<https://hal.sorbonne-universite.fr/hal-01259914>**

Submitted on 21 Jan 2016

**HAL** is a multi-disciplinary open access archive for the deposit and dissemination of scientific research documents, whether they are published or not. The documents may come from teaching and research institutions in France or abroad, or from public or private research centers.

L'archive ouverte pluridisciplinaire **HAL**, est destinée au dépôt et à la diffusion de documents scientifiques de niveau recherche, publiés ou non, émanant des établissements d'enseignement et de recherche français ou étrangers, des laboratoires publics ou privés.

# A class of morphing shell structures satisfying clamped boundary conditions

M. Brunetti<sup>a,b</sup>, A. Vincenti<sup>a</sup>, S. Vidoli<sup>b,a</sup>

<sup>a</sup> Sorbonne Univ, UPMC Univ Paris 06, CNRS, UMR 7190,  
Inst. Jean Le Rond d'Alembert, 75005 Paris, France

<sup>b</sup> Dip. Ingegneria Strutturale e Geotecnica, Univ. di Roma La Sapienza,  
Via Eudossiana 18, 00184 Rome, Italy

---

## Abstract

Many examples of multi-stable shell structures have been recently proposed with the underlying hypothesis of the shell being completely free on its boundary. We describe a class of shallow shells which are bistable after one of their sides is completely clamped. This result, which has relevant technological implications, is achieved by a suitable design of the initial, stress-free, shape.

*Keywords:* Morphing structures, Multistability, Shallow shells, Reduced models, Clamped bistable shells.

---

## 1. Introduction

Engineering structures should often be able to face several load and operating conditions; their actual shape usually stems from a compromise, after a selection of the more challenging requirements. Instead, morphing structures optimize their response to external inputs by updating their geometric configuration; despite being quite recently introduced, they could become a standard in some areas of structural engineering (as foreseen in [4]).

Here we focus on multistable shells, a particular example of morphing structures able to provide stiffness and strength whilst allowing considerable shape change. By triggering instability phenomena, or simply by exploiting displacement amplifications due to geometric nonlinearities, suitably designed shells could undergo major changes in shape under limited actuation forces.

For plates and shells, multistability can be achieved through a combination of means including pre-stresses, initial curvatures and plastic deformations.

Indeed, a competition between geometric nonlinearities and elastic properties manages the accumulation and release of elastic energy in the deformation processes and determines the equilibrium configurations, their shapes and their stability. Since stable configurations can be quite different in their geometry and the transition between them may be accomplished by different load paths, the design of multistable shells calls for mathematical models and numerical tools able to depict a *global* stability scenario., i.e., capable of providing reliable information about the number and type of stable equilibria, the energy barriers interposed between them and the most appropriate actuation strategy (for instance, one demanding a preset amount of power to the actuators). This requires simplified shell models with few degrees of freedom, so as to obtain manageable solutions and perform qualitative analysis and quick parametric studies.

For shallow shells, which are the ones typically employed in technological applications, this task is achieved by reducing the Föppl-von Kármán (FvK) shell model [6, 19] to a low-dimensional subspace ensuring a good approximation of the multiwell elastic energy [14, 18, 17]. Specifically, we use the reduction procedure introduced in [17] to infer a three-degrees-of-freedom reduced model capable of predicting the multistable behavior of suitably curved cantilever shells.

Although the reduction strategy may be applied in quite general cases, for sake of simplicity we have chosen to focus our attention on shells with rectangular planforms where only one side is actually clamped. It has to be noted that, even if boundary conditions have to be taken into account when considering a bistable shell as a component of a complex structural system, only few works deal with the design of multistable constrained shells [8, 12]. Indeed, many literature studies were limited to examine the case of shells completely free on their sides, see for instance [11, 13, 3, 7]. Instead, we are able to predict, and numerically validate, several new examples of shells that are bistable after the application of the clamp constraint. These examples are characterized by combination of geometric and material parameters within a wide range of values, thus opening the way to a proper and more general approach to design and optimization of multistable shells.

The paper is organized as follows. In section 2 we introduce the class of pseudo-conical shells. These are shallow shells, with rectangular planform, characterized by distinct curvatures, say  $h_1$  and  $h_2$ , of two opposite sides; cylindrical shells are included as the special case  $h_1 = h_2$ . This class is sufficiently large to allow some room for optimization and sufficiently simple to allow a physical insight of the bistable response. In section 3 the displacement ansatz to obtain

the reduced shell model is introduced and discussed: the hypothesis of uniform curvature, used in several literature studies, must be abandoned in order to allow more complex shell configurations. Section 4 is devoted to show the main results: in particular, we give the conditions on the design parameters for a pseudo-conical shell to be mono- or bi-stable after clamping. For shells that are bistable, aimed at providing an effective actuation of such morphing structures, we provide a method to compute an optimal path between the two equilibria. In the same section, the predictions obtained by applying the reduced 3-dofs model are confirmed by comparison with refined FE simulations. Finally in section 5 we draw some conclusions and discuss possible directions for future research.

## 2. Design parameters: natural shape and material constants

In this study a suitable choice of the natural (stress-free) configuration of the shell is sought as the primary mean to induce bistability; we do not consider here another well known source of multistable behaviors, namely the presence of inelastic pre-stresses, see [9].

While several authors already investigated natural configurations with uniform curvatures [see e.g. 14, 18, 5, 3], we abandon this simplifying hypothesis to consider more general configurations. Specifically, within the shallow shell assumption, we restrict our attention to shells with pseudo-conic natural configurations. These last can be mathematically described by surfaces in the form:

$$\mathcal{S}_0 = \{(x, y, w_0(x, y)), 0 \leq x \leq L_x, -L_y/2 \leq y \leq L_y/2\}, \quad (1)$$

with

$$w_0(x, y) = \frac{y^2}{2} \left( h_1 + (h_2 - h_1) \frac{x}{L_x} \right), \quad (2)$$

for some  $h_1, h_2 \in \mathbb{R}$  and  $0 < L_y \leq L_x$ . Figure 1 shows the meaning of these parameters and some of these shapes when the parameters  $h_1$  and  $h_2$  are varied for  $L_x = L_y$ .

The curvatures of the natural configuration are therefore not uniform and are given by:

$$h_x = 0, \quad h_{xy} = \frac{(h_2 - h_1)y}{L_x}, \quad h_y = h_1 + (h_2 - h_1) \frac{x}{L_x}. \quad (3)$$

Incidentally, cylindrical shells are included as the special case  $h_2 = h_1$ .

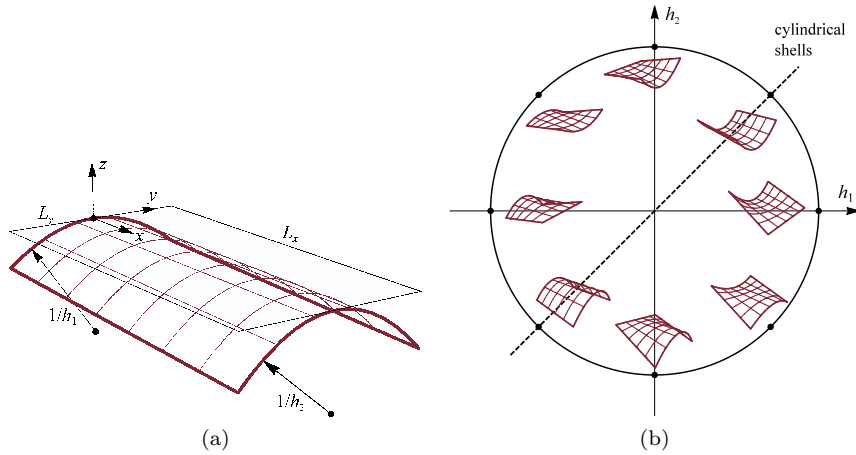


Figure 1: (a) Design parameters for the natural stress-free configuration. (b) Resulting configurations in the curvature plane  $(h_1, h_2)$  for  $L_x = L_y$ .

Three design parameters completely identify the natural shape of the shell: the aspect ratio  $\eta = L_x/L_y \geq 1$  and the curvatures  $h_1$  and  $h_2$  which can be interpreted, cfr. Fig. 1a, as the curvatures in direction  $y$  of the sides  $x = 0$  and  $x = L_x$ , respectively. As will be clear in the following, the area  $L_x L_y$  will play a role only in the scaling of curvatures based on the characteristic radius  $R$ , cfr. (25).

Concerning the constitutive properties of the material, for sake of simplicity we consider only homogeneous orthotropic shells with no coupling between bending and stretching (see [15]). Specifically, assuming the principal material directions aligned with the coordinate directions  $x$  and  $y$ , the constitutive relations between bending moments  $M$  and curvatures  $k$  will read

$$\begin{aligned} M_x &= D_{11}(k_x - h_x) + D_{12}(k_y - h_y), & M_{xy} &= D_{33}(k_{xy} - h_{xy}), \\ M_y &= D_{12}(k_x - h_x) + D_{22}(k_y - h_y), \end{aligned} \quad (4)$$

while the relations between membranal stresses  $N$  and membranal strains  $\varepsilon$  will read:

$$\begin{aligned} N_x &= A_{11}(\varepsilon_x - f_x) + A_{12}(\varepsilon_y - f_y), & N_{xy} &= A_{33}(\varepsilon_{xy} - f_{xy}), \\ N_y &= A_{12}(\varepsilon_x - f_x) + A_{22}(\varepsilon_y - f_y), \end{aligned} \quad (5)$$

where strains  $\{f_x, f_y, 2f_{xy}\}$  represent non-zero membrane stresses in the flat reference configuration, whilst curvatures  $\{h_x, h_y, 2h_{xy}\}$  provide non-zero bend-

ing moments in the reference configuration. Moreover, since we do not consider inelastic pre-stresses, the Gauss compatibility equation holds true:

$$f_{x,yy} + f_{y,xx} - 2f_{xy,xy} = h_y h_x - h_{xy}^2$$

where  $(\bullet)_{,x} = \partial(\bullet)/\partial x$ ,  $(\bullet)_{,y} = \partial(\bullet)/\partial y$ . Note that the bending moments vanish when the curvatures equal the ones in the natural configuration; similarly the membranal stresses vanish when the membranal strains equal a field which is compatible, via the Gauss compatibility equation, with the curvatures of the natural configuration.

Moreover we suppose the shells under consideration to be homogeneous through the thickness; this implies a proportionality between the membranal and bending stiffness matrices as

$$D_{11} = \frac{A_{11} t^2}{12}, \quad A/A_{11} = D/D_{11} = \begin{bmatrix} 1 & \nu & 0 \\ \nu & \beta & 0 \\ 0 & 0 & \gamma \end{bmatrix}, \quad (6)$$

for  $t$  the shell thickness. Here  $\beta = D_{22}/D_{11} = A_{22}/A_{11}$  measures the ratio between the membrane and bending stiffnesses in the coordinate directions,  $\gamma = D_{33}/D_{11} = A_{33}/A_{11}$  measures the shear and torsional moduli and  $\nu = D_{12}/D_{11} = A_{12}/A_{11}$  measures the in-plane and out-of-plane Poisson effects. For  $A$  and  $D$  to be positive definite, we must have  $\beta > \nu^2$  and  $\gamma > 0$ . In all the following the material is supposed orthotropic with  $\beta = 1$ ,  $\gamma = 0.931$  and  $\nu = 0.908$ , see [10].

### 3. Reduced nonlinear model

#### 3.1. Motivations

For shells having the natural shapes parameterized by (2), we study the stability properties once the side  $x = 0$  has been clamped. In particular our aim is to characterize the number and the nature of all such stable equilibria.

To this aim, one could, in principle, use a nonlinear finite element approximation of the shell under consideration. Starting from a meshing of the stress-free configuration  $\mathcal{S}_0$ , one should impose the clamping boundary condition on  $x = 0$  and, therefore, try to find all the possible stable equilibria, imposing and releasing suitable displacement or force fields. A similar study is not easily automated

and, actually, turns out to be extremely difficult as soon as the number of degrees of freedom becomes large: in our experience even coarse FE meshes lead to computational difficulties. We also point out that continuation techniques could fail as the equilibrium branches of similar structures often appear as turning points: thus, there is no way to continue such branches from other already known equilibria, and no guarantee for having found all the equilibria.

These difficulties motivate the use of discrete, low-dimensional models as the one introduced in [17]. Despite being based on few degrees of freedom, similar nonlinear reduced models are able to effectively describe the overall stability scenario of shallow shells, the number and type of bifurcations and their post-critical behavior.

The equilibrium equations for such reduced models of FvK shells are polynomials of order 3 in the Lagrangian parameters, see Sect. 3.3. Hence, if the number  $n$  of degrees of freedom is low, one could efficiently apply polynomial root-finding techniques that are guaranteed to give all the equilibrium branches. On a standard modern workstation, trying both the function `NSolve` in `MATHEMATICA` and the homotopy continuation method of `PHCPACK` [16], we have found that a limit condition for the discrete model could be  $n \leq 5$ . Indeed the total degree of the root-finding problem, and therefore the number of complex equilibrium branches, grows as  $3^n$ . Already for  $n = 5$  the roots are 243, but only a few of them correspond to real stable equilibria. For  $n > 5$  the time necessary to trace all the solutions exponentially increases. The numerical results discussed in the following are obtained with a discrete reduced model having  $n = 3$  degrees of freedom. *A posteriori* these results are carefully checked in terms of stability with the commercial FE software `Abaqus`.

### 3.2. Main modeling assumptions

The main assumptions of the generalized Föppl von-Kármán theory are briefly recalled for the reader's convenience, see [2].

Thin shallow shells are characterized by two small geometric parameters: the shallowness  $\sigma = L/R$  and the slenderness  $\tau = t/L$ ; here  $L$  is the characteristic dimension of the shell planform,  $R$  is the typical radius of curvature and  $t$  the shell thickness. In particular the small parameter  $\epsilon := \sigma^2 \tau^2 = t^2/R^2$  controls the ratio between bending and stretching energy.

The main kinematical assumption of the FvK theory is to seek for shell

configurations in the form

$$\mathcal{S} = \{(x + u(x, y), y + v(x, y), w(x, y)), 0 \leq x \leq L_x, -L_y/2 \leq y \leq L_y/2\}, \quad (7)$$

with a proper scaling law between the in-plane displacement fields  $u$  and  $v$  and the transverse displacement field  $w$ : specifically  $w = O(\epsilon)$  whilst  $u = O(\epsilon^2)$  and  $v = O(\epsilon^2)$ . This last assumption implies that the contributions of the in-plane and transverse displacements to the membranal strains of the surface  $\mathcal{S}$  are comparable. Namely, within an error  $O(\epsilon^4)$ , we have

$$\varepsilon_x = u_{,x} + w_{,x}^2/2, \quad \varepsilon_y = v_{,y} + w_{,y}^2/2, \quad \varepsilon_{xy} = (v_{,x} + u_{,y} + w_{,x} w_{,y})/2, \quad (8)$$

Instead the curvatures of the surface  $\mathcal{S}$  depend only the transverse displacement  $w$ ; within an error  $O(\epsilon^3)$ , one has

$$k_x = w_{,xx}, \quad k_y = w_{,yy}, \quad k_{xy} = w_{,xy}. \quad (9)$$

The stable equilibria of a FvK shell are then found as local minima of the total energy, sum of the bending and stretching elastic energies:

$$\begin{aligned} \mathcal{E}(u, v, w) = & \frac{1}{2} \int_0^{L_x} \int_{-L_y/2}^{L_y/2} (M_x k_x + M_y k_y + 2M_{xy} k_{xy}) \, dx dy \\ & + \frac{1}{2} \int_0^{L_x} \int_{-L_y/2}^{L_y/2} (N_x \varepsilon_x + N_y \varepsilon_y + 2N_{xy} \varepsilon_{xy}) \, dx dy, \end{aligned} \quad (10)$$

with the bending moments and membranal stresses given in (4) and (5).

To efficiently minimize (10), it is important to note that the in-plane displacements  $u$  and  $v$  can be solved in terms of transverse displacement  $w$  solving a linear elasticity problem. Indeed necessary conditions for the functional  $\mathcal{E}$  to be stationary with respect to  $u$  and  $v$  are

$$N_{x,x} + N_{xy,y} = 0, \quad N_{xy,x} + N_{y,y} = 0, \quad (11)$$

while for the system (8) and (9) to be integrable one must have (Gauss compatibility):

$$\varepsilon_{x,yy} + \varepsilon_{y,xx} - 2\varepsilon_{xy,xy} = k_x k_y - k_{xy}^2. \quad (12)$$

By inversion of the constitutive relations (5), (12) is transformed in terms of

stresses to get

$$A_{11}^{-1} \left[ \frac{(\beta N_x - \nu N_y)_{,yy} + (N_y - \nu N_x)_{,xx}}{\beta - \nu^2} - \frac{2}{\gamma} N_{xy,xy} \right] = (k_x k_y - k_{xy}^2) - (h_x h_y - h_{xy}^2) := \Delta g. \quad (13)$$

Equations (11) and (13) are a standard plane elasticity problem which is linear in the data, namely the difference  $\Delta g$  in Gaussian curvature between the actual and natural configurations.

### 3.3. Steps of the reduction procedure

We sketch the reduction procedure presented in [17] to deduce a discrete approximation with few degrees of freedom of the Föppl von-Kàrmàn functional (10). This procedure simply exploits the linearity of eqns. (11) and (13) to solve in terms of Lagrangian parameters the membranal problem.

*Step 1.* We introduce an *ad hoc* ansatz for the transverse displacement field. For the case under consideration, we seek  $w$  in the form

$$w(x, y) = q_1 \frac{x^2}{2} + q_2 \frac{y^2}{2} + q_3 \frac{x^3}{6} + q_4 \frac{x^2 y^2}{2} + q_5 \frac{xy^2}{2}, \quad (14)$$

uniquely defined by five Lagrangian parameters  $q_1$  to  $q_5$ .

*Step 2.* We compute explicitly the forcing term in (13). Using (9) and (14)

$$k_x = q_1 + q_3 x + q_4 y^2, \quad k_y = q_2 + q_5 x + q_4 x^2, \quad k_{xy} = q_5 y + q_4 xy, \quad (15)$$

and, therefore,

$$\begin{aligned} \Delta g = & q_1 q_2 + (q_2 q_3 + q_1 q_5) x + (q_1 q_4 + q_3 q_5) x^2 + q_3 q_4 x^3 + \\ & + \left( \frac{(h_1 - h_2)^2}{L_x^2} + q_2 q_4 - q_5^2 \right) y^2 - q_3 q_5 x y^2 - 3 q_4^2 x^2 y^2. \end{aligned} \quad (16)$$

*Step 3.* We solve the membranal problem for  $\Delta g$  given by (16). Due to the linearity of the differential problem, this account for solving the same problem for all the following seven forcing terms

$$\{1, x, x^2, x^3, y^2, xy^2, x^2 y^2\} \rightarrow \{N^{00}, N^{10}, N^{20}, N^{30}, N^{02}, N^{12}, N^{22}\}, \quad (17)$$

and then use the same linear combination, as in (16), to obtain the resulting

membranal stress field

$$N = q_1 q_2 N^{00} + (q_2 q_3 + q_1 q_5) N^{10} + (q_1 q_4 + q_3 q_5) N^{20} + q_3 q_4 N^{30} \dots \quad (18)$$

*Step 4.* We use the ansatz for the displacement (14) and the membranal solution (18) to compute the energy functional (10) in terms of Lagrangian parameters

$$\mathcal{E} \simeq \hat{\mathcal{E}}(q_1, \dots, q_5). \quad (19)$$

As the membranal stresses (18) and strains, through (5), are second-order polynomials of  $q_1, \dots, q_5$ , the approximated functional (19) is a fourth-order polynomial in the Lagrangian parameters.

### 3.4. Remarks

*Remark 1.* Assuming the transverse displacement in the form (14) allows the shell to achieve an arbitrary linear combination of the shapes shown in Fig. 2. Only the first two configurations from the left, corresponding to the Lagrangian parameters  $q_1$  and  $q_2$ , have uniform curvature.

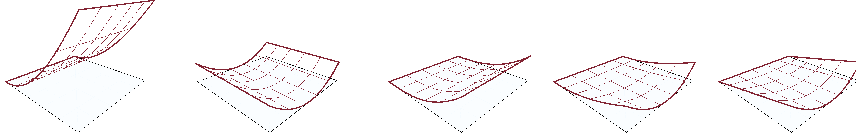


Figure 2: Base configurations in (14): for  $\eta = 1$  from left to right the shapes moduled by  $q_1, q_2, \dots, q_5$ .

The assumption (14) allows us to describe the pseudo-conical natural configurations (2) when:

$$q_1 = q_3 = q_4 = 0, \quad q_2 = h_1, \quad q_5 = \frac{h_2 - h_1}{L_x}. \quad (20)$$

Moreover, (14) allows to easily clamp the boundary  $x = 0$ . Indeed, one easily obtains

$$w(0, y) = q_2 y^2 / 2, \quad w_{,x}(0, y) = q_5 y^2 / 2, \quad (21)$$

and the clamping conditions are achieved setting both  $q_2$  and  $q_5$  to zero. In this last case, the average curvatures are controlled by  $\bar{k}_x = q_1 + L_x q_3 / 2 + L_y^2 q_4 / 12$  and  $\bar{k}_y = L_x^2 q_4 / 3$ , while  $\bar{k}_{xy} = 0$ .

*Remark 2.* For shells constrained by the clamp condition, *i.e.* within the subspace  $q_2 = q_5 = 0$ , the gaussian curvature difference (16) reduces to

$$\Delta g = q_1 q_4 x^2 + q_3 q_4 x^3 + \frac{(h_1 - h_2)^2}{L_x^2} y^2 - 3 q_4^2 x^2 y^2. \quad (22)$$

Therefore, it suffices to solve only four (out of the seven) auxiliary membranal problems (17).

*Remark 3.* The auxiliary elliptic problems (11)-(13) can be solved either in terms of Airy functions or in terms of displacements with standard FE codes. Note, however, that the precision in the evaluation of the membranal stresses  $N$  (and strains  $\varepsilon$ ) is of fundamental importance for a good estimate of the stretching energy in (19). Actually, the precision allowed by the numerical solution of the membranal problems turns out to be the key ingredient of the proposed procedure; indeed, when applying reduction techniques based on multiple ansatzs for all the displacement fields, dozens of degrees of freedom are normally required in order to reach such a high precision on membranal stresses  $N$ , see [1] or [13].

#### 4. Numerical results

The study of the stable equilibria of the pseudo-conical shells after clamping reduces to minimize the functional (19)

$$\min_{q_1, q_3, q_4} \hat{\mathcal{E}}(q_1, 0, q_3, q_4, 0; \eta, h_1, h_2) \quad (23)$$

within the three-dimensional subspace  $q_2 = q_5 = 0$  as the design parameters  $\eta$ ,  $h_1$  and  $h_2$  are varied.

In this section we present the results of such a minimization and compare them to refined FE simulations.

##### 4.1. Overall stability properties

For every choice of  $\eta$ ,  $h_1$  and  $h_2$ , the stationarity conditions for (23) are a system of three third-order polynomial equations in the unknowns  $(q_1, q_3, q_4)$ . Among all the  $3^3 = 27$  complex roots, we select the ones which are real and check their stability (minimality) through the eigenvalues of the Hessian matrix. We have found that, once clamped on one side, shells with pseudo-conical shapes described by (2) can have either one or two stable configurations.

Figure 3 displays the mono-stability (white) and bi-stability (gray) regions in the plane of design parameters  $(h_1, h_2)$  for aspect ratios  $\eta = 1, 2, 3$ , respectively. We recall that  $h_2$  is the curvature of the side  $(x = L_x)$  in the natural stress-free configuration; the opposite side  $(x = 0)$ , having curvature  $h_1$  in the natural configuration, is the one to be clamped.

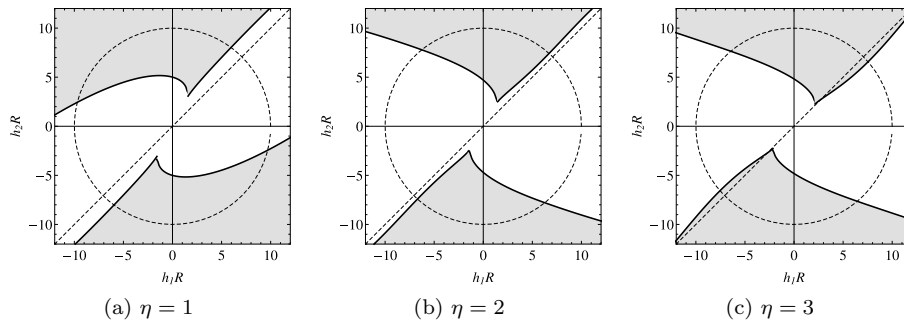


Figure 3: Monostability (white) and bistability (gray) regions in the natural curvature plane  $(h_1, h_2)$ .

We can notice the following:

- For any value of the aspect ratio, the monostability region includes a neighborhood of the origin  $h_1 \simeq h_2 \simeq 0$ ; in other words almost flat natural configurations are monostable.
- Due to the symmetry, labeling  $h_2^p(h_1, \eta)$  the lower boundary of the upper bistability region for given aspect ratio, the shells are bistable if

$$h_2 \geq h_2^p(h_1, \eta), \quad \text{or if} \quad h_2 \leq -h_2^p(-h_1, \eta). \quad (24)$$

- The threshold value for bistability  $h_2^p(h_1, \eta)$  depends on the curvature  $h_1$  of the side  $(x = 0)$ . In other words, clamping the side  $(x = 0)$  induces a stress field which is of fundamental importance to determine the bistable behaviour of the clamped shell. The larger  $h_1$  is, the larger is such stress field and the larger must be the curvature  $h_2$  of the opposite side in order for the shell to be bistable.
- Shells having natural cylindrical configurations, *i.e.* those along the dashed line  $h_1 = h_2$ , are either monostable or very close to the margin of bistability region. These shells would therefore exhibit, even if bistable, one of the two configurations with tiny stability margins.

Finally note that these results were derived from a discrete model of shallow shell; in order to satisfy this hypothesis, the curvatures should be bounded by:

$$\sqrt{h_1^2 + h_2^2} \leq 10 R^{-1}, \quad R := \sqrt{12\psi} \frac{L_x L_y}{t}, \quad \psi \simeq 3.9 \times 10^{-4} (1 - \nu^2). \quad (25)$$

This bound was obtained in [9] for a shell of isotropic material ( $\beta = 1$ ,  $\gamma = (1 - \nu)/2$ ) and  $L_x \simeq L_y$ . The bound (25) is displayed by dashed circles in Figs. 3: for natural curvatures  $(h_1, h_2)$  having norm larger than this value, the shallowness hypothesis is not fulfilled and the FvK model could progressively lose its predictivity. In other words, the conditions in (25) are needed to ensure that the shells are sufficiently shallow but not overly curved, otherwise the limits of what is meant by shallow are exceeded and a more geometrically exact analysis would be required. In particular for a shell having  $\nu \simeq 0.4$  this bound corresponds to the shallowness  $\|h\|L$  scaling as

$$\|h\|L \simeq 160 t/L;$$

for instance, if  $t \simeq 1$  mm and  $L \simeq 30$  cm, one has  $\|h\|L \simeq 0.5$ .

#### 4.2. Sample bistable configurations and energy path between them

Figures 4 and 5 give more insight on the bistable configurations and on the multi-well energy profiles achievable with pseudo-conical natural shapes.

In particular, in Fig. 4 the stability diagram of Fig. 3a is zoomed in the region  $h_1 > 0$  for  $\eta = 1$ . According to four choices of the natural configurations, labeled by points A, B, C, D in Fig. 4a and shown in Fig. 4b (red shapes), we depict the shapes of the clamped stable configurations (black shapes in Fig. 4b) and the associated energy profiles. Here, the dimensionless elastic energy is plotted against the parameter  $s$ , see (26), meaning a normalized distance between the minima.

The pseudo-conical shape corresponding to point B in the monostable region exhibits, once clamped, a convex energy profile with only one minimum. The other choices, falling within the bistability regions, are instead characterized by a double-well elastic energy. We can note that all the clamped stable configurations (black shapes in Fig. 4b) are characterized by non-vanishing energy values of their minima; the natural configurations (red shapes) are indeed the ones being stress-free.

We can note also the difference in the energy profiles corresponding to points

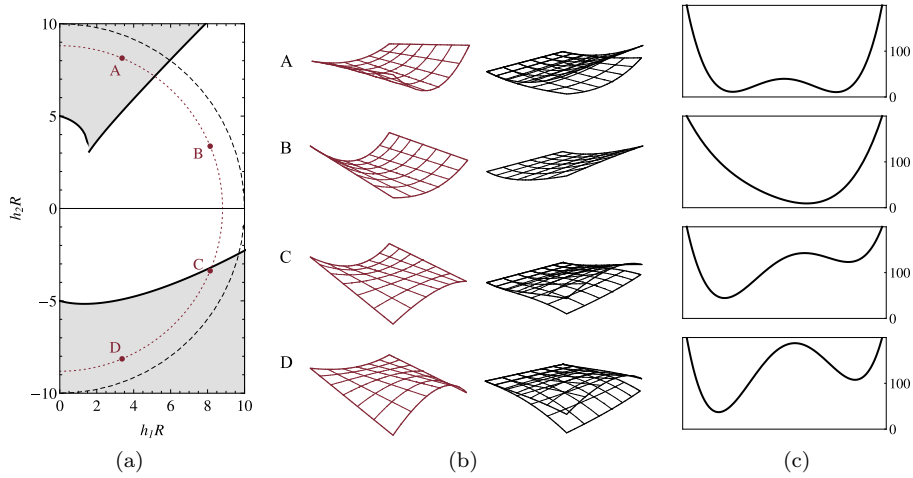


Figure 4: (a) Stability diagram within  $h_1 > 0$  for  $\eta = 1$ . (b) Natural configurations and clamped configurations for the pseudo-conical shapes A, B, C, D and (c) the associated energy profiles, where the horizontal axis is the normalized distance  $s$  along the straight line path on the energy landscape, see (26).

A, C and D. In the former case (A) the two stable equilibria are characterized by similar energy values while being separated by a relatively small energy gap. In the latter case (D) a more relevant energy gap separates the two minima which are also characterized by different values of the elastic energy. Finally, point C, chosen near the boundary of the bistability region, is characterized by a small stability margin of one of its minima. All these features become extremely important when considering the actuation problem for such clamped shells.

Figure 5 displays a similar stability scenario for more slender pseudo-conical shapes having  $\eta = 3$ . With respect to the case  $\eta = 1$ , one could notice that the point C for  $\eta = 3$  falls within the monostability region and that the energy profiles corresponding to configurations A and D are characterized by smaller energy gaps. We also point out the considerable difference between the two clamped stable configuration of point D (last row of Fig. 5b). In section 4.3 these shapes, resulting from the 3dofs reduced model, will be checked and compared to refined FE simulations.

A word of caution must be given regarding the energy profiles between minima. Indeed the ones shown in Figs. 4c and 5c refer to straight paths between the stable configurations and, therefore, they are not necessarily optimal from an energetic point of view. Specifically, labeling  $m_1$  and  $m_2$  the two minima within

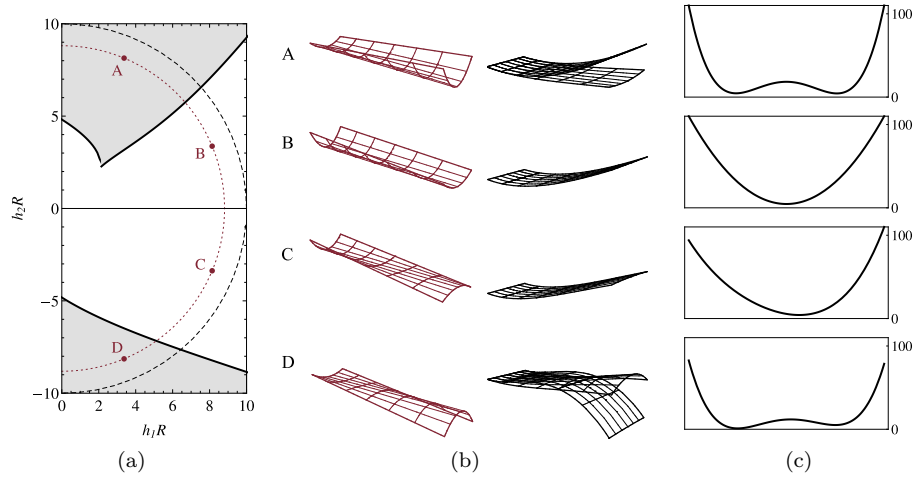


Figure 5: (a) Stability diagram within  $h_1 > 0$  for  $\eta = 3$ . (b) Natural configurations and clamped configurations for the pseudo-conical shapes A, B, C, D and (c) the associated energy profiles.

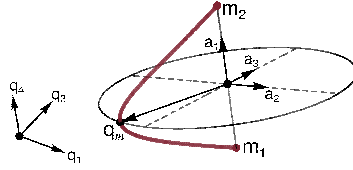


Figure 6: Construction of the optimal path between the minima  $m_1$  and  $m_2$ .

the three-dimensional space spanned by the Lagrangian parameters  $\{q_1, q_3, q_4\}$ , the straight path  $\mathbf{q}_s(s)$  is defined by

$$\mathbf{q}_s(s) = (1 - s) \mathbf{m}_1 + s \mathbf{m}_2, \quad s \in [0, 1]. \quad (26)$$

However, with reference to Fig. 6, a minimum energy path between  $m_1$  and  $m_2$  can be found as follows:

- compute the vector  $\mathbf{a}_1 = (\mathbf{m}_2 - \mathbf{m}_1)$  pointing from  $m_1$  to  $m_2$ ,
- compute, by a Gram-Schmidt process, a new orthogonal reference frame  $(\mathbf{a}_1, \mathbf{a}_2, \mathbf{a}_3)$  to express the shell configuration

$$\mathbf{q}(s, s_2, s_3) = \mathbf{m}_1 + s \mathbf{a}_1 + s_2 \mathbf{a}_2 + s_3 \mathbf{a}_3,$$

- with  $s$  fixed, call  $s_2 = \hat{s}_2(s)$ ,  $s_3 = \hat{s}_3(s)$  the solutions of the two-dimensional

	$h_1^{-1}(\text{cm})$	$h_2^{-1}(\text{cm})$	$t$ (mm)	$L_x$ (cm)	$L_y$ (cm)	$\eta$
P	21	14	1	15	15	1
Q	21	-14	1	15	45	3

Table 1: Geometric parameters for two pseudo-conical shells.

minimization problem

$$\min_{s_2, s_3} \hat{\mathcal{E}}(\mathbf{q}(s, s_2, s_3); \eta, h_1, h_2),$$

Hence, a minimum energy path connecting  $\mathbf{m}_1$  to  $\mathbf{m}_2$  is given by

$$\mathbf{q}_m(s) = \mathbf{m}_1 + s \mathbf{a}_1 + \hat{s}_2(s) \mathbf{a}_2 + \hat{s}_3(s) \mathbf{a}_3, \quad s \in [0, 1].$$

This path can be seen as the path of least resistance connecting the minima of the unloaded shell. Since it is computed starting from the elastic energy it has to be considered reliable as long as the actuation forces remain small. Clearly, since the functions  $\hat{s}_2(s)$  and  $\hat{s}_3(s)$  are not necessarily continuous,  $\mathbf{q}_m(s)$  can exhibit jumps: this is often the case for the pseudo-conical shapes under consideration.

To show such jumps, physically corresponding to standard snap-through phenomena, we consider the two pseudo-conical shells listed in Table 1.

Once plotted in the dimensionless coordinates, P falls near point A in Fig. 4a, whilst Q is close to point D in Fig. 5a.

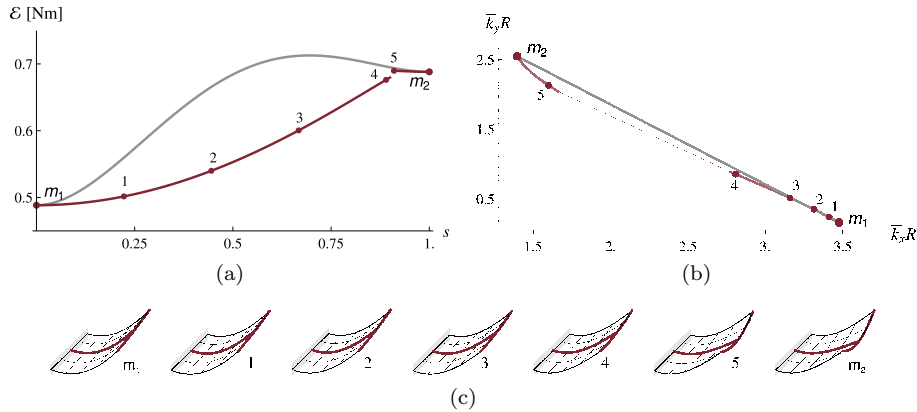


Figure 7: (a) Energy profiles of the straight (gray) and optimal (dark red) paths between the clamped equilibria of shell P. (b) Average curvatures along the same paths. (c) Shell configurations along the optimal path.

Figure 7 compares the elastic energy along the straight path  $\hat{\mathcal{E}}(\mathbf{q}_s(s))$  with the elastic energy along the optimal path  $\hat{\mathcal{E}}(\mathbf{q}_m(s))$  for the pseudo-conical shell P. Despite the optimal points 1-5 being close to the straight path in Fig. 7b, this last plot, being two-dimensional, reports only the average curvatures; a third dimension would mark the difference between the configurations of the straight and optimal paths. Clearly  $\hat{\mathcal{E}}(\mathbf{q}_s(s))$  is easily computable but gives us only an upper bound for the energy gap between the equilibria. Note also that the minimum energy path is optimal only in the three-dimensional space spanned by  $\{q_1, q_3, q_4\}$ . Considering a larger space (*i.e.* more dofs) for the shell configurations could lead to find actuation paths with lower energy gaps.

Similar conclusions can be drawn also for the energy profiles of the pseudo-conical shell Q depicted in Fig. 8. For this shell, one observes a relevant jump between the two equilibrium branches stemming from  $m_1$  and  $m_2$ : compare the shapes corresponding to the configurations 3 and 4 respectively before and after the jump.

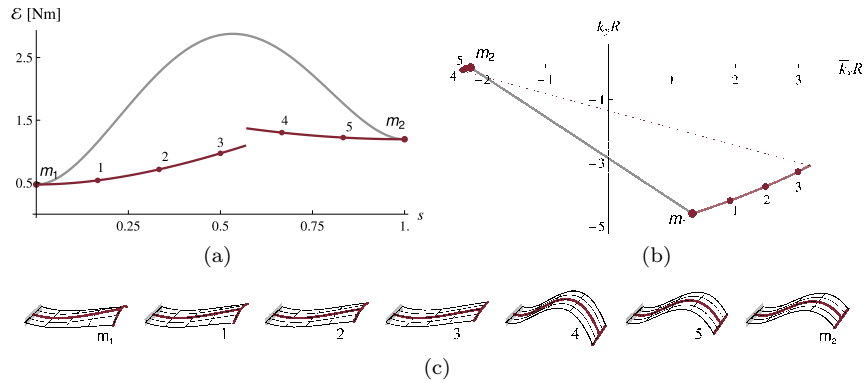


Figure 8: (a) Energy profiles of the straight (gray) and optimal (dark red) paths between the clamped equilibria of shell Q. (b) Average curvatures along the same paths. (c) Shell configurations along the optimal path.

#### 4.3. Comparison with Abaqus simulations

For several shells we have performed refined Finite Element simulations i) to check the actual existence of multiple stable configurations and ii) to compare these configurations with the ones predicted by the reduced model (23). In the following we report these results for the shells P and Q in Table 1.

Specifically the simulations have been performed in Abaqus CAE using the S4R shell elements within a fully nonlinear regime; starting from a mesh created

over the stress-free configuration we apply the clamping condition and, after convergence, we find the first stable configuration. To check the bistability, suitable displacement fields are imposed and released to check the convergence near other shapes; to this aim, the pictorial information coming from the reduced model is of fundamental importance. For each minimum found, say  $\mathbf{m}^{FE}$ , the associated elastic energy  $\mathcal{E}(\mathbf{m}^{FE})$  is computed.

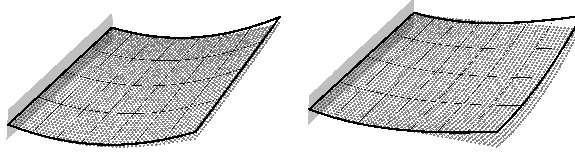


Figure 9: Clamped stable configurations for the pseudo-conical shell P: as predicted by Abaqus (black dots) and the 3dofs reduced model (solid mesh).

For the pseudo-conical shell P, despite P being close to the boundary of the bistability region in Fig. 4a, the numerical simulations have confirmed the existence of two stable equilibria after the application of the clamping condition; in Fig. 9 the resulting shapes are compared. The elastic energy of these configurations are respectively  $\mathcal{E}(\mathbf{m}_1^{FE}) = 0.72 \times \hat{\mathcal{E}}(\mathbf{m}_1) = 0.35$  Nm, and  $\mathcal{E}(\mathbf{m}_2^{FE}) = 0.53 \times \hat{\mathcal{E}}(\mathbf{m}_2) = 0.37$  Nm.

Also for the pseudo-conical shell Q we have confirmed the existence of two clamped stable equilibria. The resulting shapes are compared in Fig. 10 and respectively have elastic energies  $\mathcal{E}(\mathbf{m}_1^{FE}) = 0.63 \times \hat{\mathcal{E}}(\mathbf{m}_1) = 0.3$  Nm, and  $\mathcal{E}(\mathbf{m}_2^{FE}) = 0.84 \times \hat{\mathcal{E}}(\mathbf{m}_2) = 1.0$  Nm. We can remark the relevant agreement between the second stable equilibrium shapes (Fig.10 right).

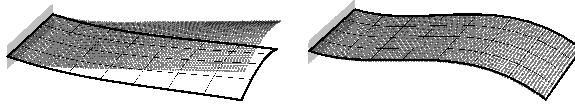


Figure 10: Clamped stable configurations for the pseudo-conical shell Q: as predicted by Abaqus (black dots) and the 3dofs reduced model (solid mesh).

In conclusion, the reduced model, having only 3 dofs against the  $10^4$  dofs used in Abaqus, systematically overestimates, within a 50% error, the energetic content of the stable configurations. Similarly the results regarding the minimum energy actuation paths and the transitional shapes between equilib-

ria should be taken only as coarse indications and, if needed, validated with more refined analyses. However, the reduced model (23) seems able to correctly estimate the existence of multiple stable configurations in the space of design parameters and to describe their shapes with sufficient approximation. Preliminary experimental evidences, not yet published, in the construction of prototypes of bistable pseudo-conical shells have confirmed the effectiveness of the reduced model predictions for design purposes.

## 5. Concluding remarks

We have reported on the problem of designing shells that are multi-stable under clamped boundary conditions. This aim has been successfully achieved tuning the curvatures of shells that are, in their stress-free configurations, pseudo-conical. We have found two compact disjoint regions in the plane of curvatures where these shells exhibit a bistable behavior: the resulting stable configurations and elastic energy profiles do depend on the actual value of the design curvatures  $(h_1, h_2)$  in Fig. 1. Two relevant examples, one for each region, have been also numerically validated by Abaqus.

Despite only considering a special case of boundary conditions (clamping only one side of the shell) and a special case of the stress-free configuration (characterized by only three design parameters), the same methods apply to more complex situations: to this aim the ansatz (14), used for deducing an effective reduced nonlinear model of the shell, should be accordingly reformulated.

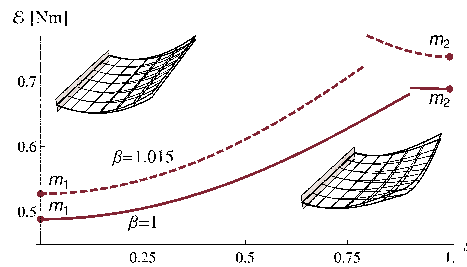


Figure 11: Tuning of the material parameters to enhance the energy gap.

In particular one could envisage both a more refined optimization of the stress-free configuration (by introducing additional design parameters) and an optimization of the material characteristics. For the latter we remark that the orthotropic nature of the material, cfr. (6), has not been exploited as the case

$\beta = 1$ , corresponding to equal Young moduli in  $x$  and  $y$  directions, has only been considered. However by a suitable tuning of the material parameters one could clearly alter both the energy gap and the energy values in the minima. In Fig. 11 the energy profile relative to the shell P is shown by a solid curve together with energy profile obtained for  $\beta = 1.015$  (dashed curve). Even such a small variation allows for a larger energy gap between  $m_1$  and  $m_2$  increasing the stability margin of the stable configuration  $m_2$ .

In conclusion, the results reported here could be considered a preliminary step toward the effective design of engineering morphing shell structures, but much more remains to be done.

### Acknowledgments

The authors acknowledge the financial support of Project ANR-13- JS09-0009 (Agence Nationale de la Recherche, 2014).

### References

- [1] S Aimmanee and M W Hyer. Analysis of the manufactured shape of rectangular thunder-type actuators. *Smart Materials and Structures*, 13(6):1389, 2004.
- [2] P G Ciarlet. A justification of the von Kármán equations. *Archive for Rational Mechanics and Analysis*, 73:349–389, 1980.
- [3] B H Coburn, A Pirrera, P M Weaver, and S Vidoli. Tristability of an orthotropic doubly curved shell. *Composite Structures*, 96:446–454, 2013.
- [4] S Daynes, P M Weaver, and J A Trevarthen. A morphing composite air inlet with multiple stable shapes. *Journal of Intelligent Material Systems and Structures*, 22(9):961–973, 2011.
- [5] A Fernandes, C Maurini, and S Vidoli. Multiparameter actuation for shape control of bistable composite plates. *International Journal of Solids and Structures*, 47(10):1449–1458, 2010.
- [6] A Föppl. *Vorlesungen über technische Mechanik*. vol.5, Leipzig, Germany. Teubner, 1907.

- [7] E Lamacchia, A Pirrera, I V Chenchiah, and P M Weaver. *Morphing shell structures: A generalised modelling approach*. *Composite Structures*, 131:1017-1027, 2015.
- [8] F Mattioni, P M Weaver and M I Friswell. *Multistable composite plates with piecewise variation of lay-up in the planform*. *International Journal of Solids and Structures*, 46(1):151-164, 2009.
- [9] W Hamouche, C Maurini, A Vincenti, and S Vidoli. Simple recipes to design and produce multistable shells. *Meccanica*, submitted.
- [10] C Maurini, A Vincenti, and S Vidoli. Modelling and design of anisotropic multistable shells. *ECCM 2010 IV European Conference on Computational Mechanics, Paris, France*, 2010.
- [11] A D Norman, K A Seffen, and S D Guest. Multistable corrugated shells. *Proceedings of the Royal Society of London A: Mathematical, Physical and Engineering Sciences*, Vol. 464(2095):1653-1672, 2008.
- [12] A S Panesar and P M Weaver. Optimisation of blended bistable laminates for a morphing flap. *Composite Structures*, 94(10), 3092-3105, 2012.
- [13] A Pirrera, D Avitabile, and P M Weaver. On the thermally induced bistability of composite cylindrical shells for morphing structures. *International Journal of Solids and Structures*, 49(5):685-700, 2012.
- [14] K A Seffen. Morphing bistable orthotropic elliptical shallow shells. *Proceedings of the Royal Society A: Mathematical, Physical and Engineering Science*, 463(2077):67-83, 2007.
- [15] P Vannucci and G Verchery. A special class of uncoupled and quasi-homogeneous laminates. *Composites Science and Technology*, 61(10):1465 - 1473, 2001.
- [16] J Verschelde. Phcpack: a general-purpose solver for polynomial systems by homotopy continuation. <http://homepages.math.uic.edu/~jan/download.html>, 2013.
- [17] S Vidoli. Discrete approximations of the Föppl - von Kármán shell model: From coarse to more refined models. *International Journal of Solids and Structures*, 50(9):1241 - 1252, 2013.

- [18] S Vidoli and C Maurini. Tristability of thin orthotropic shells with uniform initial curvature. *Proceedings of the Royal Society A: Mathematical, Physical and Engineering Science*, 464(2099):2949–2966, 2008.
- [19] T Von Kármán. *Festigkeitsprobleme im maschinenbau*. Encyklopädie der Mathematischen Wissenschaften. 1910.